Available online at www.sciencedirect.com
SCIENCE DIRECT®
Journal of Solid State Chemistry 178 (2005) 329–338
JOURNAL OF SOLID STATE CHEMISTRY
www.elsevier.com/locate/jssc

Synthesis, characterization, and photocatalytic activity for hydrogen evolution of nanocrystalline mesoporous titania prepared by surfactant-assisted templating sol–gel process

Thammanoon Sreethawong, Yoshikazu Suzuki, Susumu Yoshikawa*

Institute of Advanced Energy, Kyoto University, Uji, Kyoto 611-0011, Japan

Received 5 October 2004; received in revised form 7 November 2004; accepted 11 November 2004

Abstract

Nanocrystalline mesoporous titania was synthesized via a combined sol–gel process with surfactant-assisted templating method, treated under various calcination conditions, and evaluated for its photocatalytic activity through photocatalytic hydrogen evolution from an aqueous methanol solution. In this synthetic method, applied surfactant template molecules functioned as both mesopore-forming and gelation-assisting agents. The resulting products were methodically characterized by TG-DTA, XRD, N_2 adsorption–desorption, diffuse reflectance UV-Vis spectra, SEM, and TEM analyses. The partial phase transformation from anatase to rutile occurred beyond calcination temperature of 600 °C and anatase–rutile transition kinetics was also investigated. The calcination conditions and crystalline phases existing in the products exerted significant effect on the photocatalytic hydrogen evolution activity. The activity of the synthesized titania treated under appropriate calcination conditions was considerably higher than that of commercial titania powders, Ishihara ST-01 and Degussa P-25. It is clearly seen that the introduction of mesopore into titania photocatalyst substantially improved the photocatalytic performance.

Keywords: Sol–gel process; Surfactant-assisted template; Mesoporous titania; Photocatalysis; Hydrogen evolution; Crystallinity; Anatase phase

1. Introduction

Since the invention of photochemical water splitting over TiO_2 electrode by Fujishima and Honda [1], a multitude of studies have been focused on chemical systems that implicate the absorption of photoirradiation by chemical agents, followed by reactions leading to the splitting of water into H_2 and O_2. Since hydrogen is recognized as an environmental friendly and a highly efficient fuel, and water is also a renewable and cheap resource, the generation of H_2 by direct water splitting attainable without polluted by-products is one of potential alternatives to produce fuel for future H_2 energy supply. The utilization of oxide semiconductor photocatalyst for water splitting is among the most promising techniques because the photocatalyst is in the form of solid phase, which is relatively inexpensive, safe for operation, and resistant to deactivation.

Among oxide materials, titania (TiO_2) has been considerably investigated and shown to be very effective for technological importance including environmental pollutant cleanup and photocatalysis applications [2–5]. To date, much attention has been underlined on the photocatalytic H_2 evolution from water splitting in the presence of TiO_2 dispersion under light irradiation. Absorption of photons with energy equal or higher than the potential difference between conduction and valence band energies, so-called energy band gap, results in the formation of conduction band electrons (e^-) and accompanying valence band holes (h^+). However, H_2 cannot, in fact, be effectively produced via the splitting

*Corresponding author. Fax: +81 774 38 3508.
E-mail address: s-yoshi@iae.kyoto-u.ac.jp (S. Yoshikawa).

0022-4596/$ - see front matter © 2004 Elsevier Inc. All rights reserved.
doi:10.1016/j.jssc.2004.11.014

of water over the clean TiO_2 surface because of its large energy band gap, i.e. 3.2 eV for anatase form and 3.0 eV for rutile form, causing facile recombination of the photoinduced species. To overcome this barrier, sacrificial reagents, such as methanol, are generally used to remove the generated holes by oxidation reaction at valence band of TiO_2, while gaseous H_2 is concurrently produced from reaction between the electrons and protons in solution at the conduction band [4,6–8].

In the past decade, mesoporous materials have been of great interest as catalysts because of their unique textural and structural characteristics. Several key techniques have been adopted to prepare mesoporous TiO_2 such as sol–gel process [9], hydrothermal process [10], and ultrasonic irradiation process [11]. The use of templating materials as pore-forming agents has also been demonstrated for synthesis of highly active mesoporous TiO_2 photocatalyst [12,13]. However, the investigation on photocatalytic H_2 evolution with mesoporous TiO_2 photocatalyst has been rarely examined. Recently, our previous articles were made on the feasible utilization of nanocrystalline mesoporous TiO_2 prepared via a combined sol–gel process with surfactant-assisted templating method of laurylamine hydrochloride (LAHC)/tetraisopropyl orthotitanate (TIPT) modified with acetylacetone (ACA) system for photocatalytic H_2 evolution [14,15]. Therefore, it is worthy to obtain an insight into how various preparation conditions affect the properties of the mesoporous TiO_2 in this synthetic system, since developing simply new synthesis methods with templating materials and clarifying the role of the resulting TiO_2 in photocatalytic H_2 evolution is vital for further investigation.

In this article, the straightforward combined sol–gel process with surfactant-assisted templating method was reported as a potential technique for nanocrystalline mesoporous TiO_2 synthesis. The physical properties of the nanocrystalline mesoporous TiO_2 were thoroughly studied in relation to its photocatalytic activity of H_2 evolution. The thermal treatment effect during the preparation of the photocatalyst under various calcination conditions was principally discussed. The satisfactorily high H_2 evolution rate was attained by controlled thermal treatment conditions of the mesoporous TiO_2 compared with the prevalently used commercial TiO_2 powders, namely Ishihara ST-01 and Degussa P-25.

2. Experimental

2.1. Materials

Tetraisopropyl orthotitanate (TIPT, Tokyo Chemical Industry Co., Ltd), laurylamine hydrochloride (LAHC, Tokyo Chemical Industry Co., Ltd), and acetylacetone (ACA, Nacalai Tesque, Inc.) were used for this experiment. All chemicals were analytical grade and used without further purification. TIPT was used as a titanium precursor for mesoporous TiO_2 photocatalyst. LAHC was used as a template behaving as a mesopore-forming agent. Note that without LAHC, gelation could not have occurred, indicating that LAHC also behaved as a gel formation-assisting agent. ACA, which serves as a modifying ligand, was applied to moderate the hydrolysis and condensation processes of titanium precursor species. Commercially available TiO_2 powders, Ishihara ST-01 (Ishihara Co., Ltd.) and Degussa P-25 (Nippon Aerosil Co., Ltd.) were selected for comparative study of photocatalytic H_2 evolution.

2.2. Synthesis procedure

Nanocrystalline mesoporous TiO_2 photocatalyst was synthesized via a combined sol–gel process with surfactant-assisted templating mechanism in an LAHC/TIPT modified with ACA system. In typical synthesis, a specified amount of ACA was first introduced into TIPT with the same mole. The mixed solution was then gently shaken until intimate mixing. Afterwards, 0.1 M LAHC aqueous solution of pH 4.2 was added to the ACA-modified TIPT solution, in which the molar ratio of TIPT to LAHC was tailored to the value of 4. The mixture was continuously stirred at 40 °C overnight to obtain transparent yellow sol. Then, the gel was formed by placing the TiO_2 sol into an oven kept at 80 °C for a week. Subsequently, the gel was dried overnight at 80 °C to eliminate the solvent, which was mainly distilled water used for preparation of LAHC aqueous solution. The dried sample was calcined at 500–700 °C for 1–24 h to remove LAHC template and consequently produce the desired mesoporous TiO_2 photocatalyst.

2.3. Characterizations

Simultaneous thermogravimetry and differential thermal analysis (TG-DTA, Shimadzu DTG-50) with a heating rate of 10 °C/min in a static air atmosphere was used to study the thermal decomposition behavior of the as-prepared (dried) photocatalysts with α-Al_2O_3 as the reference. X-ray diffraction (XRD) was used to identify the structure and composition of crystalline photocatalyst. A Rigaku PMG-A2 XRD system generating monochromated Cu$K\alpha$ radiation with continuous scanning mode at the rate of 2°/min and operating conditions of 35 kV and 15 mA was used to obtain XRD patterns. A nitrogen adsorption system (BEL Japan BELSORP-18 Plus) was employed to measure adsorption–desorption isotherms at liquid nitrogen temperature of 77 K. The Brunauer–Emmett–Teller (BET) approach using adsorption data over the relative pressure ranging from 0.05 to 0.35 was utilized to

determine specific surface area. The Barrett–Joyner–Halenda (BJH) approach was used for calculation of mean pore size and pore size distribution. The sample was degassed at 200 °C for 2 h to remove physisorbed gases prior to measurement. The sample morphology was observed by a scanning electron microscope (JEOL JSM-6500FE) and a transmission electron microscope (JEOL JEM-200CX) operated at 15 and 200 kV, respectively. A Shimadzu UV-2450 UV-Visible spectrometer was exploited to record diffuse reflectance spectra of the samples at room temperature with $BaSO_4$ as the reference.

2.4. Photocatalytic H_2 evolution system

Photocatalytic H_2 evolution reaction was carried out in a closed gas-circulating system. In a typical run, a specified amount of photocatalyst was suspended in aqueous methanol solution (0.2 g photocatalyst, 20 mL CH_3OH, 200 mL distilled water) by means of a magnetic stirrer in an inner irradiation reactor made of Pyrex glass. A 300 W high-pressure Hg lamp was utilized as the light source. Prior to the reaction, the mixture was deaerated by purging with Ar gas repeatedly. To avoid the heating of the solution during the course of the reaction, water was circulated through a cylindrical Pyrex jacket located around the light source. The gaseous H_2 evolved was periodically collected and analyzed by an on-line gas chromatograph (Shimadzu GC-8A, Molecular sieve 5A, Argon gas), which was connected with a circulation line and equipped with a thermal conductivity detector (TCD).

3. Results and discussion

3.1. Photocatalyst characterizations

The nanocrystalline mesoporous TiO_2 was synthesized via the surfactant-assisted templating sol–gel process in LAHC/TIPT modified with ACA system. When TIPT was first mixed with ACA, ACA combined with Ti atom, leaving one isopropoxyl group. The coordination number of Ti atom changed from 4 to 5, causing a color change from colorless to yellow [16]. Following the mixing of ACA-modified TIPT with LAHC aqueous solution, yellow precipitates were abruptly formed due to partial hydrolysis of modified TIPT molecules. The solution was continuously stirred at 40 °C to dissolve the precipitates and acquire transparent yellow sol, which was ensued from an interaction between the hydrolyzed TIPT molecules and hydrophilic head groups of micellar LAHC and a suspension of these interacted species in the solution as infinitesimally colloidal solid particles or clusters. Afterwards, the gelation proceeded at 80 °C through a condensation process between the modified TIPT molecules attached with the LAHC head groups accompanying with the detachment of ACA as evidenced by a formation of white gel with a thin layer of transparent yellow liquid on the gel. After complete gelation for a week, the gel was dried at 80 °C in an ambient environment to attain xerogel (dried TiO_2 sample).

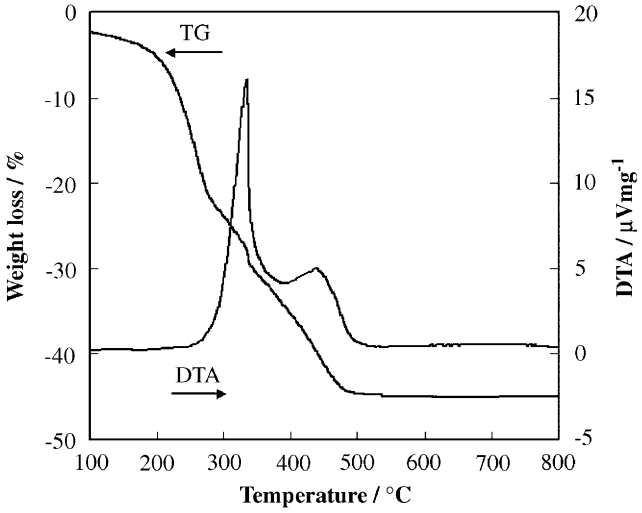

Fig. 1. TG-DTA curves of the as-synthesized TiO_2 (dried sample).

The TG-DTA curves of the dried TiO_2 are shown in Fig. 1. The DTA curve shows two main exothermic peaks. The first exothermic peak, with its maximum at 334.4 °C, is very sharp and narrow, and is attributed to the burnout of the surfactant template. The second exothermic peak, with its maximum at 438.3 °C, is weak and broad, and corresponds to the crystallization process of the photocatalyst [17]. The total weight loss measured from the TG curve was 44.91 wt%. Since the TG curve shows that weight loss ended at 500 °C, minimum calcination temperature at this value, i.e. 500 °C, was sufficient for complete removal of the organic surfactant molecules. All of the mesoporous TiO_2 samples after surfactant template removal turned from yellow (as-synthesized) to white color. To examine the effects of synthesis variables for photocatalyst preparation, calcination times were increased from 1 to 24 h at different calcination temperatures of 500, 600, and 700 °C.

The XRD patterns of TiO_2 samples in comparison with those of Ishihara ST-01 and Degussa P-25 used as TiO_2 references are shown in Fig. 2. The phase identification and approximate crystallite size of the photocatalyst from XRD analysis are summarized in Table 1. The average crystallite size was calculated from the line broadening of X-ray diffraction peak using the Sherrer formula [18] as expressed by Eq. (1):

$$L = k\lambda/\beta \cos\theta, \quad (1)$$

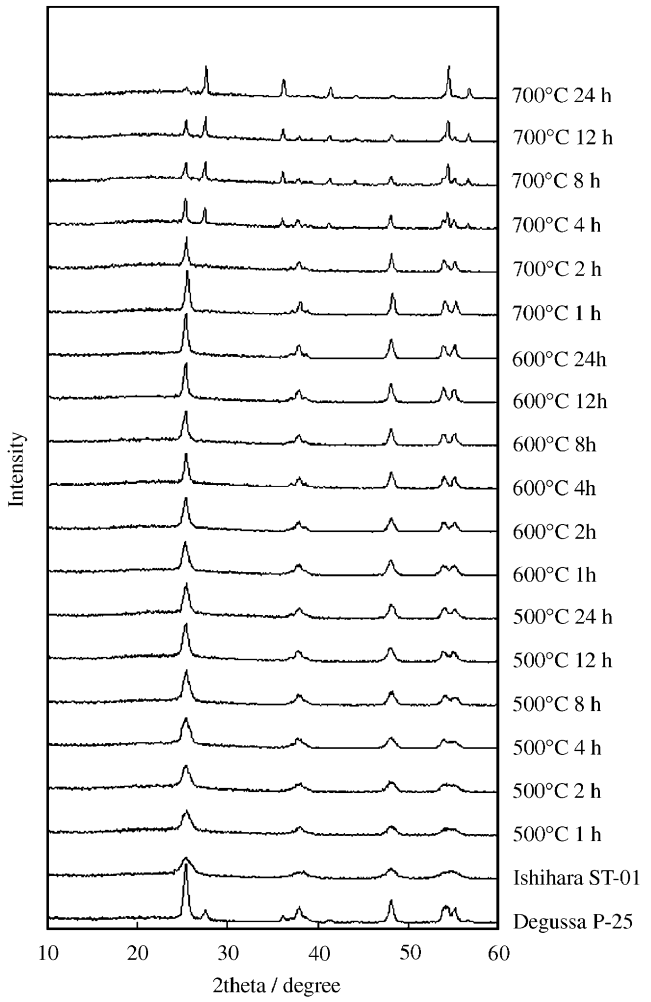

Fig. 2. XRD patterns of the mesoporous TiO_2 calcined at various conditions. Note that Ishihara ST-01 and Degussa P-25 were included for comparison.

where L is the crystallite size, k the Sherrer constant usually taken as 0.89, λ the wavelength of the X-ray radiation (0.15418 nm for Cu$K\alpha$), and β is full width half maximum (FWHM) of diffraction peak measured at 2θ.

The XRD patterns of the samples calcined at 500 and 600 °C for entire calcination time showed crystalline structure of pure anatase phase. The dominant peaks at 2θ of about 25.2, 37.9, 47.8, 53.8, and 55.0°, which represent the indices of (101), (004), (200), (105), and (2 1 1) planes respectively, are conformed to crystalline structure of anatase phase. However, at calcination temperature of 500 °C, the crystallization to anatase phase of the synthesized materials was not fully developed even at calcination time of 24 h in comparison with ones calcined at 600 °C. The calcination temperature of 600 °C was determined as the highest limit for yielding well-crystallized pure anatase phase TiO_2 produced by this synthetic system. At calcination temperature of 700 °C, partial phase transformation from anatase to rutile was observed, resulting in the combination of anatase and rutile phases. The occurrence of the dominant peaks at 2θ of about 27.4°, 36.1°, 41.2°, and 54.3°, which correspond to the indices of (110), (101), (111), and (211) planes respectively, indicates the presence of rutile phase in the materials at this calcination temperature. The rutile ratio (W_R) in terms of weight fraction was estimated from XRD intensity data by using Eq. (2) [19]:

$$W_R = [1 + 0.8 I_A / I_R]^{-1}, \quad (2)$$

where I_A and I_R represent integrated intensities of anatase (101) and rutile (110) diffraction peaks, respectively. All calculated numbers of rutile ratio are also included in Table 1. The rutile content increased from 15 to 78% with increasing calcination time from 1 to 24 h. The anatase–rutile transition kinetics of the mesoporous TiO_2 prepared by the present system can also be obtained by consideration of the isothermal change in rutile content in the materials calcined at this temperature. Due to the model of Avrami for nucleation and growth kinetics, the basic generalized Avrami equation can be expressed by Eq. (3) [20]:

$$\mathrm{Ln}[-\mathrm{Ln}(1 - W_R)] = n\,\mathrm{Ln}(t) + \mathrm{Ln}(k), \quad (3)$$

where W_R is the rutile ratio, t the calcination time, n the transition kinetics order, and k the transition kinetics constant. The generalized Avrami plot between $\mathrm{Ln}[-\mathrm{Ln}(1 - W_R)]$ and $\mathrm{Ln}(t)$ is shown in Fig. 3. The correlation revealed a straight line with a slope equal to 0.68, which seems to obey the first-order kinetics for anatase–rutile phase transition. The result is comparatively similar to the work reported by Ha et al. [21]. Furthermore, it is clearly seen that regardless of the phase present, prolongation of thermal treatment conditions by increasing both calcination temperature and calcination time resulted in higher crystallinity, indicating the grain growth of TiO_2 crystallites as shown in Table 1.

The N_2 adsorption–desorption isotherms of the synthesized materials exhibited typical IUPAC type IV pattern with the presence of H2 hysteresis loop as exemplified in Fig. 4 for the sample calcined at 600 °C for 4 h, which provided the highest photocatalytic H_2 evolution activity as discussed later. The hysteresis loop is typically ascribed to the existence of mesopores in the products. A sharp increase in adsorption volume of N_2 was observed and located in the P/P_0 range of 0.6–0.9. This sharp increase can be assigned to the capillary condensation, indicating good homogeneity of the sample and fairly small pore size since the P/P_0 position of the inflection point is pertained to pore dimension. As illustrated in the inset of Fig. 4, the pore size distribution obtained from this combined surfactant-assisted sol–gel process is quite narrow, verifying good quality of the samples. Moreover, the isotherms revealed a single and

Table 1
Summary of XRD analysis of the synthesized mesoporous TiO_2, Ishihara ST-01, and Degussa P-25

Material	Calcination temperature/°C	Calcination time/h	Phase from XRD pattern	Rutile ratio, W_R	Crystallite size/nm	
					Anatase(101)	Rutile(110)
Synthesized TiO_2	500	1	Anatase	—	10.3	—
		2	Anatase	—	10.5	—
		4	Anatase	—	12.3	—
		8	Anatase	—	13.6	—
		12	Anatase	—	14	—
		24	Anatase	—	15.5	—
Synthesized TiO_2	600	1	Anatase	—	15.5	—
		2	Anatase	—	17.1	—
		4	Anatase	—	20.7	—
		8	Anatase	—	21.3	—
		12	Anatase	—	22.5	—
		24	Anatase	—	24	—
Synthesized TiO_2	700	1	Anatase + rutile	0.15	25.2	40.5
		2	Anatase + rutile	0.24	28.2	41.1
		4	Anatase + rutile	0.47	32.2	43.3
		8	Anatase + rutile	0.57	33	44.7
		12	Anatase + rutile	0.59	33.7	45
		24	Anatase + rutile	0.78	35.5	44.5
Ishihara ST-01	—	—	Anatase	—	10.4	—
	600	4	Anatase	—	20	—
Degussa P-25	—	—	Anatase + rutile	0.23	20.7	29.9

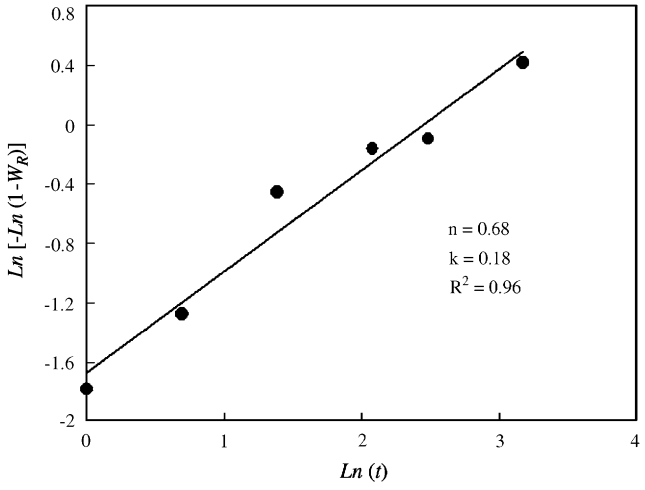

Fig. 3. Generalized Avrami plot of isothermal change in rutile content for transition kinetics study.

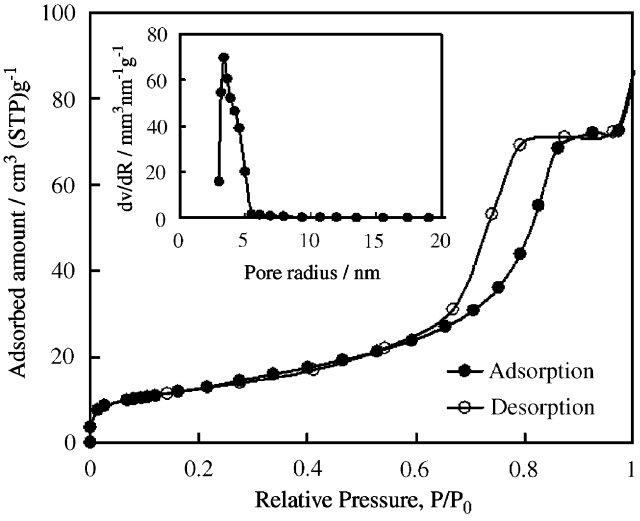

Fig. 4. N_2 adsorption–desorption isotherm and pore size distribution (inset) of the nanocrystalline mesoporous TiO_2 calcined at 600 °C for 4 h.

well-defined step and a clear hysteresis loop in the desorption branch, pointing out some diffusion bottlenecking in the pore structure. The experimental results on BET surface area, mean pore diameter, and total pore volume of all synthesized materials are shown in Table 2. As obviously seen, the surface area decreased from 122 to 68 $m^2 g^{-1}$, from 70 to 21 $m^2 g^{-1}$, and from 29 to 3 $m^2 g^{-1}$ with increasing calcination time from 1 to 24 h at calcination temperature of 500, 600, and 700 °C, respectively. With increasing both calcination time and temperature, the observed loss in surface area is attributable to pore coalescence due to the crystallization of walls separating mesopores. Subsequently, this tendency caused an increase in mean pore diameter and a decrease in total pore volume of the bulk materials, as expected.

Typical SEM and TEM images of the material calcined at 600 °C for 4 h are shown in Fig. 5. SEM image in Fig. 5(a) indicates that the TiO_2 nanoparticles are reasonably uniform in size with some

Table 2
Summary of N_2 adsorption–desorption results of the synthesized mesoporous TiO_2, Ishihara ST-01, and Degussa P-25

Material	Calcination temperature/°C	Calcination time/h	BET surface area/$m^2 g^{-1}$	Mean pore diameter/nm	Total pore volume/$cm^3 g^{-1}$
Synthesized TiO_2					
	500	1	121.5	5.06	0.242
		2	105.8	6.76	0.235
		4	100.9	6.34	0.216
		8	85.3	6.76	0.196
		12	82.4	7.22	0.197
		24	68.3	8.38	0.171
Synthesized TiO_2					
	600	1	69.7	6.34	0.164
		2	58.2	6.34	0.146
		4	46.4	6.76	0.142
		8	40.8	7.22	0.129
		12	40.9	8.38	0.128
		24	21.2	10.98	0.082
Synthesized TiO_2					
	700	1	29.4	6.76	0.094
		2	16	6.76	0.055
		4	4.5	7.22	0.027
		8	3.4	7.76	0.033
		12	3.8	9.94	0.023
		24	2.9	12.24	0.018
Ishihara ST-01					
	—	—	300	—[a]	—[a]
	600	4	76.4	—[a]	—[a]
Degussa P-25	—	—	51.6	—[a]	—[a]

[a] N_2 adsorption–desorption isotherm corresponds to IUPAC type II pattern.

nanoagglomerates of 3–4 crystallites. The presence of mesopore could be clearly observed by SEM analysis. In addition, TEM image in Fig. 5(b) demonstrates the formation of highly crystalline TiO_2 aggregates composed of three-dimensional disordered primary nanoparticles. The average size of the TiO_2 nanoparticles is approximately 20 nm, which is consistent with the crystallite size estimated from XRD analysis. Therefore, each particle observed by TEM analysis should be a single crystal.

The diffuse reflectance UV-Vis spectra of the samples calcined at various conditions were analyzed to estimate their energy band gap by using the Kabelka-Munk function, $F(R)$ as expressed by Eq. (4) [22]:

$$F(R) = (1 - R)^2/2R, \quad (4)$$

where R is ratio of the reflected light intensity to the reflected light intensity of the reference. Fig 6(a) represents the plots of $F(R)$ as a function of wavelength of the samples calcined at 500 and 600 °C for 4 h. The energy band gap (E_g, eV) is determined by extrapolating of the onset of the rising part to x-axis (λ_g, nm) of the plots as shown by the dotted line and calculation by Eq. (5):

$$E_g = 1240/\lambda_g, \quad (5)$$

The band gap of the samples calcined at temperatures lower than 700 °C, i.e. 500 and 600 °C, for the entire range of the investigated calcination times is approximately 3.2 eV ($\lambda_g = 387$ nm), corresponding to the energy band gap of anatase TiO_2. However, the band gap of the samples calcined at 700 °C for various calcination times varies with the rutile ratio (W_R). Fig. 6(b) shows the plots of $F(R)$ as a function of wavelength of the samples calcined at this temperature. From the calculation, the band gap gradually decreases from anatase TiO_2 band gap of 3.2 eV ($\lambda_g = 387$ nm) at calcination time of 1 h ($W_R = 0.15$), to 3.06 eV ($\lambda_g = 405$ nm) at calcination time of 2 h ($W_R = 0.24$), and finally to rutile TiO_2 band gap of 3.0 eV ($\lambda_g = 413$ nm) at calcination time equal or higher than 4 h ($W_R \geqslant 0.5$). These results imply that the significantly low rutile content less than 15% exerts negligible influence in altering the band gap from anatase to rutile TiO_2, whereas the moderate rutile content between 15 and 50% exerts partial influence in such an alteration and the high rutile content of more than 50% completely alters the band gap characteristic from anatase to rutile TiO_2. As comparatively seen from Fig. 6(a) and (b), it is perceptible that the light-absorption capability of anatase TiO_2 at near UV

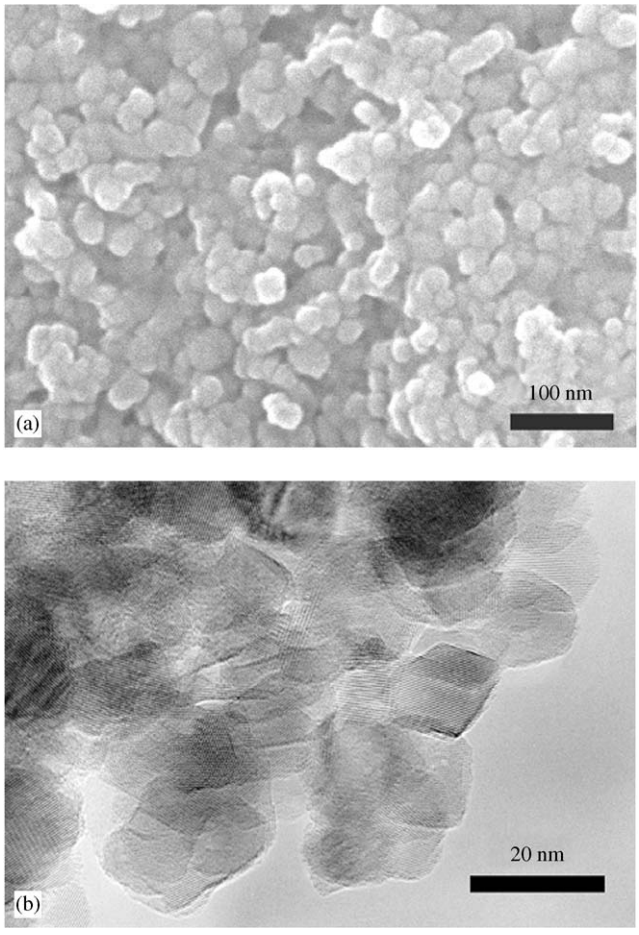

Fig. 5. (a) SEM and (b) TEM images of the mesoporous TiO_2 photocatalyst calcined at 600 °C for 4 h.

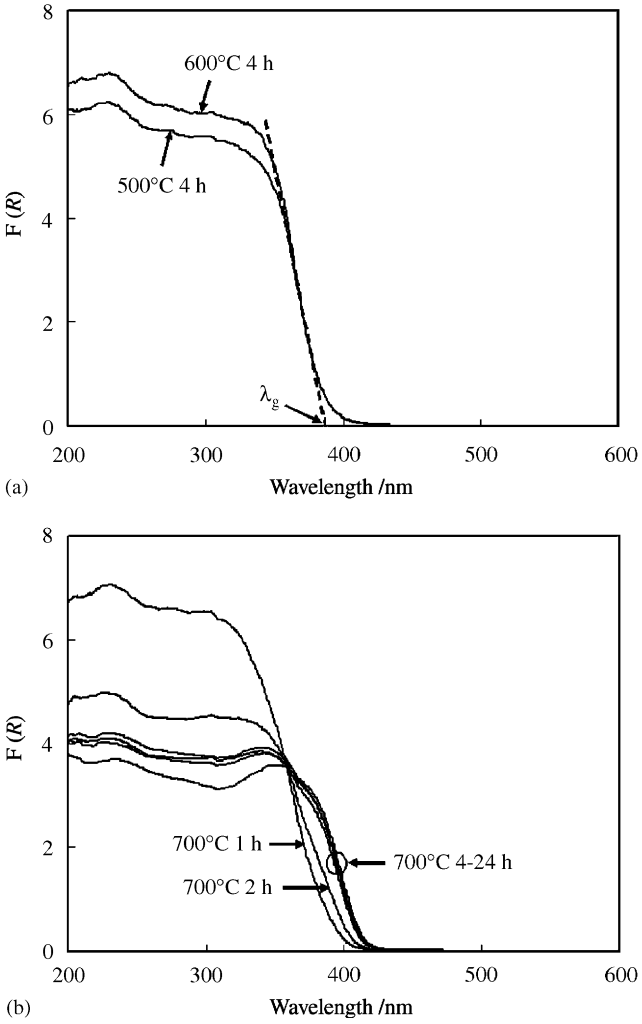

Fig. 6. Diffuse reflectance UV-Vis spectra of the mesoporous TiO_2 calcined at (a) 500 and 600 °C for 4 h and (b) 700 °C for various calcination times.

region is significantly higher than that of rutile TiO_2 [23]. Furthermore, it should be noted that the TiO_2 particle size from this synthetic system (more than 10 nm) is somewhat too large to observe the evidence of quantum confinement effect, resulting in the absence of the blue shift of the absorption onset.

3.2. Photocatalytic H_2 evolution

The photocatalytic H_2 evolution from aqueous methanol solution was studied as a probe photochemical reaction over the as-synthesized nanocrystalline mesoporous TiO_2 calcined at various calcination conditions compared with commercial Ishihara ST-01 and Degussa P-25 TiO_2 powders. No appreciable H_2 evolution was detected in the absence of either light irradiation or photocatalyst. However, in the presence of both, detectable H_2 evolution was observed. This therefore confirms that gaseous H_2 evolved was in fact generated from photocatalyzed water splitting over the photocatalysts. The results on the amount of H_2 evolved from the mesoporous TiO_2 are illustrated in Fig. 7. The photocatalytic H_2 evolution rates from Ishihara ST-01 and Degussa P-25 at identical reaction conditions are 83.9 and 30.8 $\mu mol\,h^{-1}$ (not shown in the figure), respectively, while the highest photocatalytic H_2 evolution from the mesoporous TiO_2 treated with optimum thermal treatment conditions of 600 °C for 4 h was observed at the rate of 330.5 $\mu mol\,h^{-1}$. In comparison with the photocatalytic activity, the mesoporous TiO_2 provided much significantly higher H_2 evolution than both commercial TiO_2 powders. Despite large surface area about 300 $m^2\,g^{-1}$ of Ishihara ST-01, imperfect crystallization from XRD data (Fig. 2) accompanying with fairly small crystallite size (Table 1) is considered to favorably increase the probability of mutual e^-/h^+ recombination at both surface and bulk traps. In case of Degussa P-25, the phase combination between anatase and rutile (rutile ratio of 0.23 as shown in Table 1) might be the cause of very low photocatalytic activity as

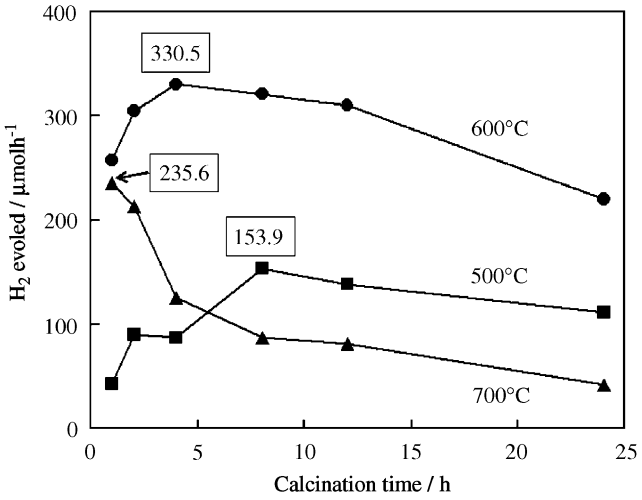

Fig. 7. Dependence of the amount of H_2 evolved on calcination times at various calcination temperatures (500, 600, and 700 °C): 0.2 g photocatalyst, aqueous methanol solution (20 mL CH_3OH, 200 mL H_2O), irradiation time 5 h. Note that the H_2 evolution rates by Ishihara ST-01 and Degussa P-25 were 83.9 and 30.8 μmol h^{-1}, respectively.

described later. Moreover, lack of mesoporous structure in both commercial TiO_2 powders (as shown in Table 2) is also subjected to less reactant accessibility for the photocatalytic reaction. In contrast, the use of the nanocrystalline mesoporous TiO_2 with uniform pore size and high crystallinity could decrease the number of lattice defects and then facilitate the electron transport for reacting with water molecule adsorbed at TiO_2 surface along the mesopore structure. To further demonstrate the importance of mesoporosity, Ishihara ST-01 was brought to calcination process at 600 °C for 4 h, which are the optimum thermal treatment conditions for the mesoporous TiO_2. Characterizations and photocatalytic activity test of calcined Ishihara ST-01 were performed for comparison. It was found from XRD analysis that crystalline phase was preserved as anatase TiO_2 with higher crystallinity due to the sharper peak, and crystallite size was calculated by Sherrer formula to be 20.0 nm, which is approximately two times higher than that of uncalcined Ishihara ST-01 (Table 1). The BET surface area significantly decreased after calcination to 76.4 m^2 g^{-1} (Table 2). The H_2 evolution rate also dramatically decreased to only 7.39 μmol h^{-1}. In addition to the lack of mesoporosity but in spite of higher crystallinity of the calcined Ishihara ST-01, the large crystallite size resulting in higher probability of mutual e^-/h^+ recombination as well as great decrement in the surface area resulting in very low surface active reaction sites may be the causes of extremely low photocatalytic activity. As a consequence of these results, the mesoporosity has been proven to be very important property of TiO_2 photocatalyst. Therefore, introducing mesoporous framework into the TiO_2, especially with the proposed surfactant-assisted templating sol–gel process, is of great significance to obtain superior textural properties, leading to much better photocatalytic performance.

As can be seen from Fig. 7, the results indicated that the photocatalytic H_2 evolution activity considerably depended on calcination time. At calcination temperatures of 500 and 600 °C, the maximum H_2 evolved was observed at optimum calcination time of 8 and 4 h, respectively. The explanations can be assorted into two parts, namely, prior to and behind the highest values. Firstly, in spite of larger surface area of the materials calcined at shorter calcination times prior to the peak (i.e. 1, 2, and 4 h in case of 500 °C; 1 and 2 h in case of 600 °C), the higher amount of H_2 that evolved at longer calcination time implied that crystallinity plays a more significant role in the photocatalytic H_2 evolution activity. It was mentioned that higher crystallinity has been evaluated to drastically affect the higher photocatalytic activity of TiO_2 materials [12,24]. When increasing calcination time, smaller surface area was achieved, whereas higher crystallinity was conversely observed. By taking into account the balance of these two conflicting factors that affect photocatalytic activity, the expected increment of the photocatalytic activity owing to the increase in crystallinity (less number of lattice defects) may exceed the expected decrement of the photocatalytic activity owing to the decrease in the surface area. In second part, after the peak, the amount of H_2 evolved decreased with increasing calcination times. It could be concluded that the surface area of the synthesized TiO_2 materials predominantly governed the photocatalytic H_2 evolution activity in this range, although higher crystallinity due to prolonged calcination time was attained. Generally, prolongation of thermal treatment brought about a loss of mesopores to a great extent, and consequently, lower surface area. The decrease in surface area resulted in the less number of active surface reaction sites and subsequently less accessibility of the reactant, water molecule, to adsorb onto the photocatalyst surface, react with the photogenerated electron, and produce the gaseous H_2. For better clarity of these explanations, the photocatalytic H_2 evolution activity of the mesoporous TiO_2 materials synthesized at all thermal treatment conditions is depicted as a function of their surface areas in Fig. 8. On the contrary, the H_2 evolution over materials calcined at 700 °C gradually decreased with increasing calcination time. This may be attributed to the negatively coupled effect of the decrease in surface area and the presence of a greater extent of rutile phase. The influence of rutile content, which exerted a negative effect on the photocatalytic activity, will be discussed later.

The calcination temperature also played an important role in the photocatalytic H_2 evolution. The investigated

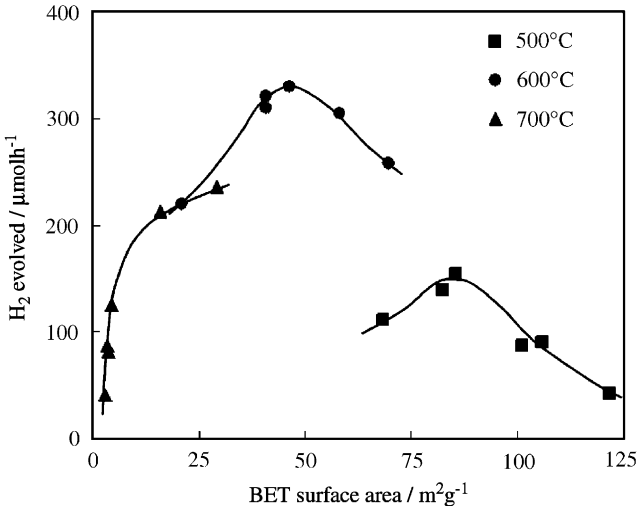

Fig. 8. Correlation between surface area of the TiO_2 photocatalysts prepared at various calcination temperatures and the amount of H_2 evolved.

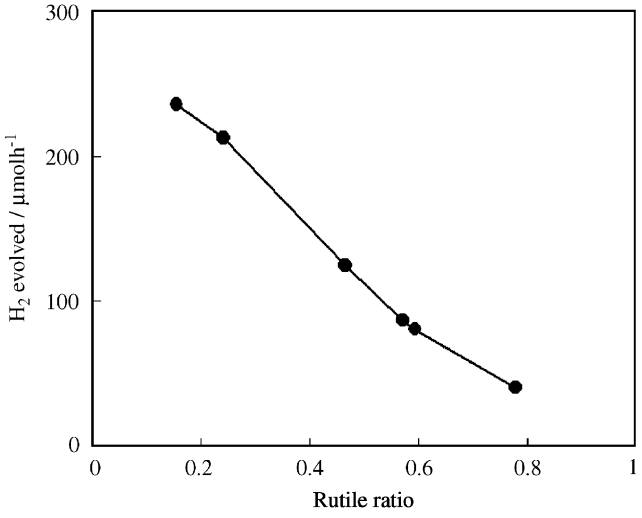

Fig. 9. Effect of rutile content in the TiO_2 photocatalysts calcined at 700 °C on the amount of H_2 evolved.

calcination temperatures for removal of surfactant template were 500, 600, and 700 °C. Among these three calcination temperatures, H_2 evolution activity reached the maximum value at calcination temperature of 600 °C for the entire range of calcination time as shown in Fig. 7. It could be inferred that although surface area of the materials calcined at 600 °C was smaller than that at 500 °C, perfect crystallization of anatase phase from a close inspection of XRD patterns is intensely considered as a major advantage. The amorphous phase contained to some extent in the materials calcined at 500 °C dramatically played a negative effect on the photocatalytic activity of H_2 evolution. It has been indicated that amorphous phase can behave as recombination centers for the photoinduced e^-/h^+ pairs. Amorphous portions have been assessed to be substantial surface and bulk traps, because they usually comprise numerous defects, i.e., impurities, dangling bonds, and microvoids [20].

As shown in Fig. 2, the phase transformation of the TiO_2 photocatalysts occurred beyond the calcination temperature of 600 °C. The influence of rutile phase content in the samples on the photocatalytic activity was therefore investigated using the materials calcined at 700 °C for various calcination times. The dependence of photocatalytic H_2 evolution upon rutile ratio is illustrated in Fig. 9. It was obviously seen that the amount of evolved H_2 gradually decreased as the rutile ratio increased. This may be attributed to the negatively coupled effect of the decrease in surface area and the presence of rutile phase. The results affirm the point that the presence of rutile phase in TiO_2 caused detrimental effect on photocatalytic activity, which is in good agreement with several reported literatures [3,23,25]. By considering the location of the conduction band level, the decrement in the photocatalytic activity could be ascribed to a lower flat band potential of rutile existing at almost similar level to the NHE potential (H^+/H_2 level), whereas that of anatase is shifted cathodically by approximately 0.2 eV. As a result, in the case of anatase TiO_2, a driving force for water reduction is sufficiently available, while a driving force for water reduction in the case of rutile TiO_2 is very small. Moreover, less light-absorption capability of rutile TiO_2 near the UV region, as clearly seen from Fig. 6, is also attributable to less photocatalytic activity for H_2 evolution than anatase TiO_2.

Overall, this study has revealed that this combined sol–gel process with surfactant-assisted template opened up a promising candidate for synthesis of nanocrystalline TiO_2 with mesopore-scaled structure with efficiently high photocatalytic activity for H_2 evolution. For this synthetic system, it should be noted that the crystallinity and crystal structure chiefly govern the photocatalytic H_2 evolution activity rather than the surface area of the TiO_2 photocatalyst. Hence, by taking into account the balance of these two conflicting intrinsic properties, i.e. crystallinity and surface area, it is crucial for high photocatalytic activity to control thermal treatment conditions leading to high crystallinity of anatase phase without formation of rutile phase.

4. Conclusions

This study was focused on using nanocrystalline mesoporous TiO_2 synthesized via a combined sol–gel process with surfactant-assisted template for efficient H_2 evolution from the photocatalytic cleavage of water. The utilization of the as-synthesized nanocrystalline

mesoporous TiO_2 thermally treated under suitable conditions promoted remarkably higher H_2 evolution in comparison with Ishihara ST-01 and Degussa P-25. The crystallinity of anatase phase materials was improved with increasing calcination temperature and partly transformed from anatase to rutile phase beyond 600 °C. The anatase–rutile phase transition of the products calcined at 700 °C was proven to obey the first-order kinetics. However, the photocatalytic activity decreased with increasing the rutile phase content. The high crystallinity of anatase phase with mesoporous structure obtained from controlled thermal treatment conditions was attributable to enhance the photocatalytic activity of H_2 evolution. In addition, the surfactant-assisted templating sol–gel process was verified as a potential approach for synthesis of nanocrystalline mesoporous TiO_2 possessing exceptionally high photocatalytic performance.

Acknowledgments

This work was financially supported by the Grant-in-aid for Scientific Research from the Ministry of Education, Science, Sports, and Culture, Japan, under the 21COE program. Grateful acknowledgments are forwarded to Prof. S. Isoda and Prof. H. Kurata at Institute for Chemical Research, Kyoto University for their continuous support of TEM apparatus.

References

[1] A. Fujishima, K. Honda, Nature 238 (1972) 37–38.
[2] O. Legrini, E. Oliveros, A.M. Braun, Chem. Rev. 93 (1993) 671–698.
[3] M.R. Hoffmann, S.T. Martin, W. Choi, D.W. Bahnemann, Chem. Rev. 95 (1995) 69–96.
[4] A.L. Linsebigler, G. Lu, J.T. Yater Jr., Chem. Rev. 95 (1995) 735–758.
[5] A. Mills, S.L. Hunte, J. Photochem, Photobiol. A: Chem. 108 (1997) 1–5.
[6] A. Kudo, K. Domen, K. Maruya, T. Onishi, Chem. Phys. Lett. 133 (1987) 517–519.
[7] T. Abe, E. Suzuki, K. Nagoshi, K. Miyashita, M. Kaneko, J. Phys. Chem. B 103 (1999) 1119–1123.
[8] S. Yin, J. Wu, M. Aki, T. Sato, Int. J. Inorg. Mater. 2 (2000) 325–331.
[9] K.M.S. Khalil, M.I. Zaki, Powder Technol. 120 (2001) 256–263.
[10] S. Kambe, K. Murakoshi, T. Kitamura, Y. Wada, S. Yanagida, H. Kominami, Y. Kera, Sol. Energ. Mat. Sol. C 61 (2000) 427–441.
[11] J.C. Yu, J. Yu, L. Zhang, W. Ho, J. Photochem. Photobiol. A: Chem. 148 (2002) 263–271.
[12] V.F. Stone Jr., R.J. Davis, Chem. Mater. 10 (1998) 1468–1474.
[13] Q. Dai, L.Y. Shi, Y.G. Luo, J.L. Blin, D.J. Li, C.W. Yuan, B.L. Su, J. Photochem. Photobiol. A: Chem. 148 (2002) 295–301.
[14] T. Sreethawong, Y. Suzuki, S. Yoshikawa, Technical Digest: The 14th International Photovoltaic Science and Engineering Conference, vol. 1, 2004, pp. 409–410.
[15] T. Sreethawong, Y. Suzuki, S. Yoshikawa, Int. J. Hydrogen Energy, in press.
[16] C.J. Brinker, G.W. Scherer, Sol–Gel Science, Academic Press, New York, 1989.
[17] D.C. Hague, M.J. Mayo, J. Am. Ceram. Soc. 77 (1994) 1957–1960.
[18] B.D. Cullity, Elements of X-ray Diffraction, Addison-Wesley Pub. Co., Reading, MA, 1978.
[19] R.A. Spurr, H. Myers, Anal. Chem. 29 (1957) 760–762.
[20] C.N.R. Rao, K.J. Rao, Phase Transitions in Solids: An Approach to the Study of the Chemistry and Physics of Solids, McGraw-Hill, New York, London, 1978.
[21] P.S. Ha, H.J. Youn, H.S. Jung, K.S. Hong, Y.H. Park, K.H. Ko, J. Colloid Interf. Sci. 223 (2000) 16–20.
[22] Y.I. Kim, T.E. Mallouk, J. Phys. Chem. 96 (1992) 2879–2885.
[23] K.E. Karakitsou, X.E. Verykios, J. Phys. Chem. 97 (1993) 1184–1189.
[24] B. Ohtani, Y. Ogawa, S. Nishimoto, J. Phys. Chem. B 101 (1997) 3746–3752.
[25] S. Ichikawa, R. Doi, Thin Solid Films 292 (1997) 130–134.